Contents lists available at ScienceDirect

Digital Chinese Medicine

journal homepage: http://www.keaipublishing.com/dcmed

Integrated plasma and synovial membrane lipidomic profiling revealing the therapeutic effects of moxibustion in collagen-induced arthritis rat models

Jiamin WEN[a], Rui ZHANG[b], Danwen WANG[a], Zhiling SUN[a]*

a. School of Nursing, Nanjing University of Chinese Medicine, Nanjing, Jiangsu 210023, China

b. Emergency Management Department, Nanjing Emergency Medical Center, Nanjing, Jiangsu 210003, China

ARTICLE INFO

Article history
Received 12 October 2024
Accepted 07 April 2025
Available online 25 June 2025

Keywords
Lipidomics
Moxibustion
Rheumatoid arthritis
Collagen-induced arthritis
Plasma
Synovial membrane
UHPLC-Q-Exactive Orbitrap MS

ABSTRACT

Objective To reveal the therapeutic effects of moxibustion in collagen-induced arthritis (CIA) rat models using the combined analysis of plasma and synovial membrane lipidomic profiling and to enhance the understanding of how moxibustion affects lipid metabolism in rheumatoid arthritis (RA).

Methods A total of 32 male Sprague-Dawley (SD) rats were randomly assigned to four groups: control, moxibustion control (MC), model, and moxibustion model (MM) groups, with 8 rats in each group. CIA was induced in SD rats by two immunizations. The paw volume was measured before the induction of CIA. Following induction, after assessing paw volume and arthritis index (AI) scores, the MC and MM groups received treatment at bilateral Shenshu (BL23) and Zusanli (ST36) acupoints for 10 min per acupoint. The intervention included three treatment courses, each spanning 6 d and followed by a 1-d interval. Paw volume and AI scores were assessed after each treatment course. After the completion of the three treatment courses, serum, plasma, synovial tissue, and ankle joint samples were collected. Enzyme-linked immunosorbent assay (ELISA) was employed to quantify the levels of interleukin (IL)-6 and tumor necrosis factor (TNF)-α in serum. Hematoxylin and eosin (HE) staining was performed for histopathological examination of the ankle joint tissues. Meanwhile, ultra-high-performance liquid chromatography coupled with Q-Exactive Orbitrap mass spectrometry (UHPLC-Q-Exactive Orbitrap MS) was utilized to analyze the plasma and synovial tissue samples. In addition, multivariate statistical analysis was performed to identify differential lipid metabolites, and Kyoto Encyclopedia of Genes and Genomes (KEGG) pathway enrichment analysis was applied to explore metabolic pathways modulated by moxibustion therapy.

Results No significant difference in hind paw volume and AI scores was observed among the groups ($P > 0.05$). After CIA induction, model group showed increased hind paw volume and AI scores compared with control group ($P < 0.05$), which were significantly reduced after moxibustion treatment in MM group compared with model group ($P < 0.05$). The levels of IL-6 and TNF-α were significantly higher in model and MM groups compared with control group ($P < 0.05$), but were lower in MM group than those in model group ($P < 0.05$). Histopathological analysis showed improved cartilage and reduced inflammation in MM group. A total of 33 differential lipid metabolites in the plasma and 24 in the synovial membranes of CIA rat models were identified when compared with control group. Among these lipid metabolites, 31 in the plasma and all 24 in the synovial membranes were regulated by moxibustion treatment.

*Corresponding author: Zhiling SUN, E-mail: szl@njucm.edu.cn.

Peer review under the responsibility of Hunan University of Chinese Medicine.

DOI: 10.1016/j.dcmed.2025.05.010

Citation: WEN JM, ZHANG R, WANG DW, et al. Integrated plasma and synovial membrane lipidomic profiling revealing the therapeutic effects of moxibustion in collagen-induced arthritis rat models. Digital Chinese Medicine, 2025, 8(2): 254-266.

Pathological analysis revealed upregulation of diacylglycerol (DG) and fatty acid (FA) levels, alongside downregulation of lysophosphatidylcholine (LPC), phosphatidylcholine (PC), and phosphatidylethanolamine (PE). Under physiological conditions, the treatment specifically reduced LPC and PC levels. Pathway enrichment analysis revealed that moxibustion predominantly affected α-linolenic acid, glycerophospholipid, and sphingolipid metabolism under pathological conditions. Under physiological conditions, the regulation was centered around α-linolenic acid and glycerophospholipid metabolism.

Conclusion The RA rat models exhibited significant lipid metabolic disturbances. Moxibustion alleviated paw swelling, reduced AI scores, modulated inflammatory cytokine levels, and partially corrected the altered levels of multiple lipid metabolites. The potential metabolic pathways implicated in the regulation of lipid metabolism under both physiological and pathological conditions include α-linolenic acid, glycerophospholipid, and sphingolipid metabolism.

1 Introduction

Rheumatoid arthritis (RA) is a chronic systemic autoimmune joint disease characterized by persistent synovitis, which can result in irreversible destruction of joints, disability, reduced quality of life, and socioeconomic burden [1]. It affects approximately 1% – 2% of the global population [2]. Currently, medication is the primary treatment for RA, including disease-modifying anti-rheumatic drugs (DMARDs), nonsteroidal anti-inflammatory drugs (NSAIDs), glucocorticoids, and biological agents. However, medication can cause toxic and adverse reactions, such as gastrointestinal side effects, abnormality in the liver, kidney damage, and infection risk [3]. Thus, treatment for RA with fewer side effects and better curative effects is urgently needed.

At present, an alternative medicine, namely traditional Chinese medicine (TCM), shows unique advantages of fewer side effects and good clinical efficacy in the prevention and treatment of RA. Moxibustion, as an important component of TCM, is one of the research hotspots in RA treatment in recent years [4]. A growing number of animal experiments has indicated that moxibustion could activate immune response, inhibit inflammatory responses, and alleviate cartilage degradation and bone destruction to lessen the severity of RA [5-7]. Clinical trials have shown that moxibustion could play anti-inflammatory and analgesic roles to improve patients' clinical symptoms and mitigate disease severity [8]. Although moxibustion has a good curative effect, limited information is known about its specific therapeutic mechanism in the treatment of RA. TCM is characterized as a multi-target, multi-system, multi-link, and multi-faceted treatment for RA [9]. Therefore, the underlying mechanism of moxibustion in the treatment of RA should be explained from the perspective of holistic science.

Metabolomics, an emerging technology in systems biology, has been applied to understand metabolic changes in endogenous metabolites in living systems in response to pathological stimuli or drug treatments to identify potential biomarkers in biological samples, such as plasma, urine, or membrane [10]. Metabolomics embodies the characteristics of integrity and dynamics, consistent with the theory of TCM [11]. In addition, it has been widely used to explore the mechanisms of both complementary and alternative medicines, which include moxibustion treatment [6]. Lipidomics, the most cutting-edge branch of metabolomics, can screen and discover endogenous small-molecule differential lipids and identify potential biomarkers in human bodies. Changes in lipid metabolism participate in the pathogenesis and disease severity of RA [12]. For example, lipid peroxidation leads to the formation of malondialdehyde, which accelerates bone erosion in RA patients and plays a critical role in the pathogenesis of RA [13]. Abnormal lipid metabolism is commonly observed in RA patients, with significantly higher levels of pro-inflammatory high-density lipoproteins (pi-HDL) compared to healthy controls. The anti-inflammatory and antioxidant functions of pi-HDL are impaired in RA patients, which are associated with disease activity [14]. In recent years, studies have shown that RA is related to different lipid metabolites and lipid metabolism pathways [15, 16]. Lipidomics based on liquid chromatography-mass spectrometry (LC-MS) is a powerful tool used to discover biomarkers in RA patients.

Although some studies have explored the therapeutic effects of moxibustion on RA patients, the understanding of its mechanism focuses primarily on localized changes at the cellular and molecular levels, lacking a systematic analysis at the metabolic level. There is a significant gap between the research regarding the role of lipid metabolism and the treatment of RA with moxibustion. Lipids, as essential components of cell membranes and key molecules in signal transduction, play important roles in inflammatory responses and immune regulation in human bodies. However, current research has predominantly concentrated on changes in cytokines or gene expression, neglecting the overall changes in the

lipid metabolism network. Hence, the advent of lipidomics technology can address this issue by comprehensively analyzing lipid metabolites in biological samples and revealing dynamic changes in metabolic pathways, thereby providing a new perspective for a deeper understanding of the therapeutic mechanisms of moxibustion treatment.

This study aimed to explore changes in lipid metabolism within the plasma and synovial membranes of RA rats using lipidomics technology, determine the potential metabolic pathways of moxibustion in the treatment of RA, and reveal the underlying therapeutic mechanism.

2 Materials and methods

2.1 Reagents and instruments

2.1.1 Reagents Reagents for establishing CIA rat models included bovine type II collagen (CII, Chondrex, USA), complete Freund's adjuvant (CFA, Sigma-Aldrich, USA), and incomplete Freund's adjuvant (IFA, Sigma-Aldrich, USA). Glacial acetic acid (Nanjing Chemical Reagent Co., Ltd., China, purity: 99.5%) was also used in the study. For the moxibustion treatment, smokeless moxa sticks (Nanyang Hanyi Aijiu Co., Ltd., Henan, China, specification: 4 mm × 120 mm) were employed. Rat interleukin (IL)-6 and tumor necrosis factor (TNF)-α enzyme-linked immunosorbent assay (ELISA) kits (Nanjing Jinyibai, China) were used for cytokine tests. The organic solvents, which included formic acid, ammonium formate, acetic acid, ammonium acetate, methanol, ethanol, and methyl tert-butyl ether (MTBE), were all of mass spectrometry (MS) grade purity and were sourced from Merck (Darmstadt, Germany). The internal standards for lipid analysis comprised lysophosphatidylethanolamine (LPE 17:1), phosphatidylethanolamine (PE 17:0/17:0), and sphingomyelin (SM 17:0) all purchased from Avanti Polar Lipids, USA. Other specific lipid standards included CUDA (Aladdin Biochemical Technology Co., Ltd., China), fatty acids (FA) 22:4, 22:5, and 22:6, and lysophosphatidylcholine (LPC 16:0) (all from Yeon Yeon Biotechnology Co., Ltd., China).

2.1.2 Instruments In this experiment, we utilized the following key instruments and equipment: D-160 handheld homogenizer (Beijing Dalong Xingchuang Company, DLAB D-160), toe volume meter (Chengdu Taimeng Software Co., Ltd., PV-200), electronic balance with a precision of 0.000 1 g (Mettler Toledo, ME155DU), and high-speed refrigerated centrifuge (Eppendorf, 5810R). Additionally, we employed high-performance liquid chromatography (HPLC, Dionex Corporation, U3000), quadrupole-Orbitrap mass spectrometer (Thermo Fisher Scientific, Q-Exactive), triple quadrupole liquid chromatography-mass spectrometer (Thermo Fisher Scientific, TSQ Vantage), vacuum centrifugal concentration machine (Thermo Fisher Scientific, Savant SPD1010), vortex mixer (Scientific Industries, Vortex-Genie 2), ultrasonic cleaner (Kunshan Ultrasonic Instruments Co., Ltd., KQ-500B), electronic balance with a precision of 0.000 1 g (Sartorius, CPA225D), and ultrapure water system (Millipore, Milli-Q).

2.2 Animals

A total of 32 specific pathogen-free (SPF) grade male Sprague-Dawley (SD) rats (7 weeks old, weighing 180 – 220 g) were purchased from Shanghai Slack Laboratory Animal Co., Ltd. [experimental animal license No. SYXK (Hu)-2017-0005], with facility license No. SYXK (Su) 2023-0077. All animals were housed in an SPF animal experiment center under controlled environmental conditions (temperature: 22 – 24 °C; humidity: 55% – 57%) with a standardized 12 h light/dark cycle. Food and water were provided ad libitum. This experiment was approved by the Animal Ethics Committee of Nanjing University of Chinese Medicine (202001A009).

2.3 Experimental design

2.3.1 Grouping and timeline The timeline of the experimental design is shown in Figure 1. After adaptive feeding for one week (day 0), hind paw volume was measured from all rats to ensure consistent initial status between groups. Subsequently, 16 out of the 32 rats were randomly divided into control group (n = 8) and moxibustion control (MC) group (n = 8), while the remaining 16 rats were used for CIA modeling. After successful establishment of CIA rat models, hind paw volume and arthritis index (AI) scores were assessed (day 14). The rats were randomly divided into model group (n = 8) and moxibustion model (MM) group (n = 8).

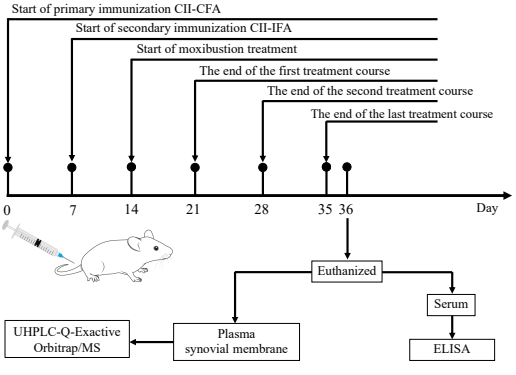

Figure 1 Timeline of the experimental design

2.3.2 CIA model establishment and evaluation In the study, CIA rat models were established in accordance with the procedures described in our previous study [6]. CII was dissolved in 0.05 mol/L glacial acetic acid to produce a 2 mg/mL mixture, which was stored at 4 °C for

12 h. Next, an equal volume of CFA was employed to prepare CII-CFA emulsion of 1 mg/mL, which was injected intradermally into rats at a dose of 0.2 mg/kg through their tails as the primary immunization. On day 7 after the first injection, another CII was again emulsified with IFA in a 1 : 1 ratio (v/v) to produce the CII-IFA emulsion, which was injected into rats at a dose of 0.1 mg/kg as the secondary immunization. Additionally, rats in control and MC groups were injected with the same volume of physiological saline at the same time points and locations. The standard of CIA model established was evaluated based on the AI scores, which were scored as follows. 0 points: no macroscopic signs of arthritis or swelling (normal state); 1 point: mild swelling limited to individual digits; 2 points: moderate redness and swelling localized to the ankle; 3 points: redness and swelling extending to the entire paw and digits; 4 points: severe inflammation involving multiple joints across the limb. CIA rats were deemed successfully modeled if the AI score for each paw was $\geqslant 2$ [17].

2.3.3 Moxibustion treatment Rats in MM and MC groups received moxibustion treatment on day 14 using a previously described method [6]. The rats were immobilized in the prone position, with their heads and limbs fixed using a customized fixation device. The hair around the acupoints was shaved to expose the skin surface for sterilization prior to moxibustion. For moxibustion, bilateral Shenshu (BL23) and Zusanli (ST36) acupoints were selected according to *Experimental Acupuncture Science* [18]. Shenshu is located 7 mm outward from the second lumbar vertebra, and Zusanli is located about 5 mm below the fibular head of the lower lateral knee joint. Each smokeless moxa stick (4 mm in diameter and 120 mm in length) was ignited and placed 2 cm above the acupuncture points for 10 min. Each rat was treated with moxibustion for three treatment courses, with each treatment course lasting 6 d, followed by a 1-d interval. Rats in control and model groups were fixed with the same method at the same time without any intervention.

2.4 Sample collection and processing

At the end of the moxibustion treatment, rats were fasted for 12 h. Then, anesthesia was induced via intraperitoneal injection of 3% pentobarbital sodium at a dosage of 50 mg/kg. Blood samples were extracted from the abdominal aorta of each rat, and centrifuged at 3 000 rpm for 10 min at 4 °C to separate serum and plasma. The serum was stored at – 80 °C for cytokine detection using the ELISA method, while the plasma was stored at – 80 °C for lipidomics analysis. Following blood collection, the skin of the left knee joint was prepared, and the patellar ligaments of both sides were longitudinally incised. The upper edge of the patella was transversely cut to the femur, creating an area of approximately 3 cm × 3 cm centered on the knee joint. The free distal patella and surrounding tissues were carefully collected using ophthalmic forceps. The synovial tissue and fibrous layer of the joint capsule were separated with ophthalmic pliers and scissors to isolate the synovial membranes. The isolated synovial membranes were stored at – 80 °C for lipidomics analysis. Additionally, the right ankle joints of the rats were removed and fixed in 4% paraformaldehyde solution for histopathological examination. All collected samples were processed and stored under specified conditions to ensure reproducibility for subsequent experiments.

2.5 Outcome measurements

2.5.1 Physical parameters Following the primary immunization, the hind paw volume of rats in the four groups were measured using a plethysmometer (PV-200, Techman Soft). Measurements were taken on the primary immunization day (day 0), on the day before moxibustion treatment (day 14), and at the end of each treatment course (day 21, 28, and 35). The measurement process lasted across the three treatment courses. The AI score was used weekly to evaluate the severity of arthritis in rats in model and MM groups, with measurement times aligning with those for hind paw volume measurements, starting from the onset of moxibustion. All parameters were evaluated by two observers independently and blinded for any data. A double-blinded method was used in the entire experiment.

2.5.2 Inflammatory markers The levels of pro-inflammatory cytokines such as IL-6 and TNF-α in the serum were measured using ELISA kits according to the manufacturer's instructions.

2.5.3 Histopathological examination At the end of the experiment, all rats were euthanized to acquire synovial membrane tissues from their right ankles. The collected tissues were fixed in 4% neutral buffered formalin for 48 h. Following fixation, the samples were dehydrated through a graded series of ethanol solutions (75%, 85%, and 95%), with each concentration being applied for approximately 1 h. The dehydrated tissues were then cleared in xylene to remove residual ethanol and embedded in paraffin blocks. The paraffin-embedded tissue blocks were sectioned into 5 μm thick slices using a microtome. The sections were mounted onto glass slides and immersed in xylene to remove paraffin. After paraffin removal, the sections were rehydrated through a descending ethanol series (100%, 95%, and 75%), with each concentration being applied for approximately 30 min. The rehydrated sections were stained with hematoxylin and eosin (HE) for 5 min and rinsed with tap water to remove excess stains. The stained sections were subsequently differentiated using 1% hydrochloric acid in 70% ethanol for 20 s to

enhance staining contrast and clarity, followed by rinsing with tap water. The sections were then blued in an alkaline solution and re-stained with HE for 2 min. The re-stained sections were dehydrated in 100% ethanol, cleared in xylene, and mounted with a glycerol-gelatin medium. After drying, the samples were examined under an optical microscope to capture synovitis and cartilage destruction in each slide.

2.6 Lipidomics analysis

2.6.1 Sample preparation and ultra-high-performance liquid chromatography (UHPLC)-MS/MS analysis Plasma samples were thawed at 4 °C, after which 20 μL of it was mixed with 225 μL of cold methanol containing internal standards, vortexed for 30 s, followed by the addition of 750 μL of precooled MTBE and oscillation at 4 °C for 10 min. Next, after being added with 188 μL of ultrapure water, the mixture was vortexed for 20 s, centrifuged at 14 000 rpm for 2 min at 4 °C. The post-centrifugation supernatant was dried and reconstituted with 110 μL of methanol : toluene (9 : 1, v/v) for subsequent analysis. Quality control (QC) samples, prepared by pooling 20 μL from each plasma sample, were injected after every eight samples to monitor instrument stability. Synovial samples were thawed at 4 °C, homogenized with 200 μL ultrapure water, and processed similarly to plasma for analysis.

Lipidomics analysis was performed using UHPLC (ultimate 3000 system) coupled with a Q-Exactive Orbitrap mass spectrometer. Plasma samples were separated on an ACQUITY CSH C18 column (2.1 mm × 100 mm, 1.7 μm) at 65 °C with a flow rate of 0.3 mL/min. The mobile phases in positive ion mode were acetonitrile: water in a 6 : 4 ratio with 0.01 mol/L ammonium formate and 0.1% formic acid (A), and isopropanol : acetonitrile in a 9 : 1 ratio with 0.01 mol/L ammonium formate and 0.1% formic acid (B), with a gradient elution (all ratios are in volume, v/v). In negative ion mode, ammonium acetate was used to replace the ammonium formate. Synovial membrane samples were analyzed under similar conditions but at a flow rate of 0.6 mL/min and adjusted gradient times. Mass spectrometry parameters included spray voltages of 3.5 kV (+) and 3.0 kV (–), with an Orbitrap resolution of 35 000 (215 – 1 800 m/z) for full scan and 17 500 (200 – 2 000 m/z) for ddMS2 mode.

2.6.2 Data processing The raw spectrogram file was converted into Abf format by Abf Converter (http://www.reifycs.com/AbfConverter/). MS-DIAL software v4.60 and the LipidBlast database were employed to analyze raw data. The data in positive ion and negative ion modes were imported into MS-DIAL for data processing, including peak detection, deconvolution identification, and alignment. For accurate mass and MS/MS matching, the public built-in LipidBlast library was used for lipid identification. Lipid information included the name of the identified lipid, retention time, mass-to-charge ratio (m/z), and peak height. The data were then exported from MS-DIAL for further statistical analysis.

The exported data matrix consisting of normalized peak areas, charge-mass ratio, retention time, and sample name was imported into MetaboAnalyst 5.0 (http://www.metaboanalyst.ca/) for further principal component analysis (PCA), partial least-squares discriminant analysis (PLS-DA), and orthogonal partial least squares discriminant analysis (OPLS-DA) to obtain an overview of the samples and identify biomarkers. Differential lipids were identified based on a variable importance in the projection (VIP) score > 1 and statistically significant differences ($P < 0.05$) in the *t* test between the model group and the control group. The effects of moxibustion intervention on lipid metabolism pathways were analyzed using MetaboAnalyst 5.0.

Hierarchical clustering and heatmap visualization were conducted using GraphPad Prism v9.4.0 based on fold-change values ($\log_2$ transformed), with Euclidean distance and Ward's linkage method applied for clustering. The identification of significantly altered pathways was based on the criteria of pathway impact > 0.1 and $-\log_{10} P > 2$. These thresholds were selected to ensure biological relevance and statistical robustness. The resulting pathways were visualized using bubble plots and network diagrams to elucidate potential therapeutic mechanisms.

2.7 Statistical analysis

Statistical analyses were performed using SPSS 22.0. Continuous variables were expressed as mean ± standard deviation (SD). After assessing normality, one-way analysis of variance (ANOVA) was conducted, followed by least significant difference (LSD) post-hoc test for homogeneous variances or Dunnett's post-hoc test for heterogeneous variances. $P < 0.05$ was considered statistically significant.

3 Results

3.1 Physical, biochemical, and histopathological evaluation of moxibustion treatment

The hind paw volume, AI scores, and the levels of IL-6 and TNF-α were evaluated to study the effects of moxibustion treatment on CIA rats. No significant differences in paw volumes and AI scores were observed among the groups ($P > 0.05$). Following CIA induction, the AI scores of rats in model and MM groups significantly increased ($P < 0.05$), reaching the threshold for successful CIA model establishment. Additionally, the hind paw volumes of

these rats also significantly increased ($P < 0.05$), further indicating the progression of arthritis (Figure 2A). Following moxibustion treatment, the hind paw volumes of rats in MM group were significantly reduced compared with model group ($P < 0.05$). Similarly, AI scores in MM group progressively decreased post moxibustion treatment and were significantly lower compared with model group ($P < 0.01$) (Figure 2B).

Histopathological examination results are shown in Figure 2C. In model group, cartilage erosion, synovial membrane proliferation, and inflammatory cell infiltration were observed, while these symptoms were alleviated in MM group, indicating that moxibustion effectively relieved joint damage and inflammation. In contrast, both control and MC groups displayed intact hyaline cartilage and smooth joint capsules, with histopathological features consistent with normal joint architecture.

Furthermore, the levels of IL-6 and TNF-α in model group were significantly higher than those in control and MC groups ($P < 0.05$) (Figure 2D). After moxibustion treatment, these inflammatory factor levels in MM group significantly decreased ($P < 0.05$), confirming the inhibitory effect of moxibustion on inflammatory responses and demonstrating its therapeutic benefits in the treatment of CIA rats.

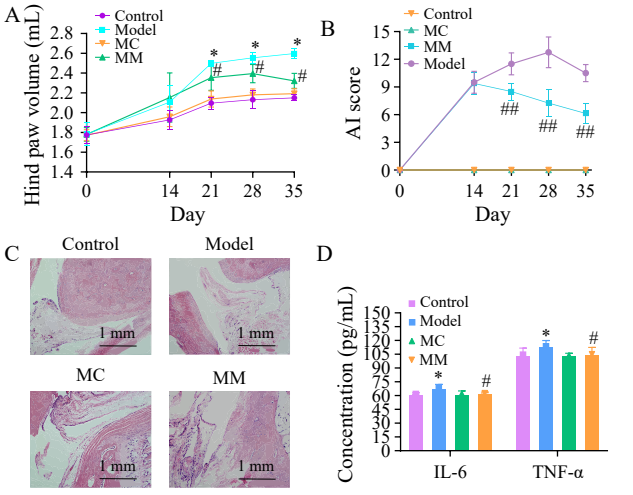

Figure 2 Evaluation of CIA model construction and therapeutic efficacy of moxibustion

A, hind paw volumes. B, AI scores. C, representative histopathological images of right ankle joints (HE staining, 100 ×). D, quantification of IL-6 and TNF-α levels in the serum. Data were represented as mean ± SD ($n = 8$). $^{*}P < 0.05$, compared with control group. $^{\#}P < 0.05$ and $^{\#\#}P < 0.01$, compared with model group.

3.2 Multivariate statistical analysis of lipid profile alterations

PCA and PLS-DA were employed to evaluate differences in lipid profiles of plasma and synovial membrane samples among different groups. The PCA score plots showed that the QC samples formed tight clusters without observable drift in both positive and negative ion modes, confirming excellent stability and repeatability of the LC-MS system throughout the analytical process (Figure 3A and 3B). Furthermore, PLS-DA analysis revealed significant separations among different groups: the lipid profiles of plasma and synovial membrane samples in model group were significantly altered, showing clear distinction from control group (Figure 3C – 3J). This significance was evident in different ion modes, specifically, in plasma samples, $P = 0.002$ in the positive ion mode and $P = 0.007$ in the negative ion mode; in synovial membrane samples, $P = 0.005$ in the positive ion mode and $P = 0.004$ in the negative ion mode. The lipid profiles in MM group were closer to those in control and MC groups, indicating that moxibustion intervention effectively alleviated the metabolic disorders caused by CIA.

To further identify differential lipids, OPLS-DA was used. OPLS-DA score plots showed significant differences in both plasma and synovial membrane samples between model group and control group (Figure 3K – 3R). The model parameters (R^2Y and Q^2) indicated good explanatory and predictive power for both plasma ($R^2Y = 0.951$, $Q^2 = 0.86$ in positive ion mode; $R^2Y = 0.991$, $Q^2 = 0.849$ in negative ion mode) and synovial membrane samples ($R^2Y = 0.964$, $Q^2 = 0.664$ in positive ion mode; $R^2Y = 0.993$, $Q^2 = 0.843$ in negative ion mode). These results demonstrated that the lipid profiles were markedly altered in CIA rats, whereas moxibustion intervention effectively regulated these changes and restored normal lipid metabolism.

3.3 Differential lipid metabolites regulated by moxibustion treatment

In plasma and synovial membrane samples, a total of 33 and 24 differential metabolites were identified in model and control groups, respectively. These differential metabolites were primarily concentrated in several key lipid classes, including DG, LPC, PC, and TG. In the pathological conditions, MM group modulated 31 differential lipid metabolites compared with model group, including upregulating the levels of DG and FA, and downregulating the levels of LPC, PC, and PE. Under physiological conditions, MC group modulated the levels of 23 differential metabolites compared with control group, including downregulating the levels of LPC and PC, further supporting the regulatory effect of moxibustion intervention (Supplementary Table S1 and S2).

In synovial membrane samples, 18 differential lipid metabolites were detected in the positive ion mode and 6 in the negative ion mode (Supplementary Table S3 and S4). The results suggested that moxibustion regulated metabolic disorders in CIA rat models. Moreover, 2 classes of lipid metabolites, namely, DG and FA, were

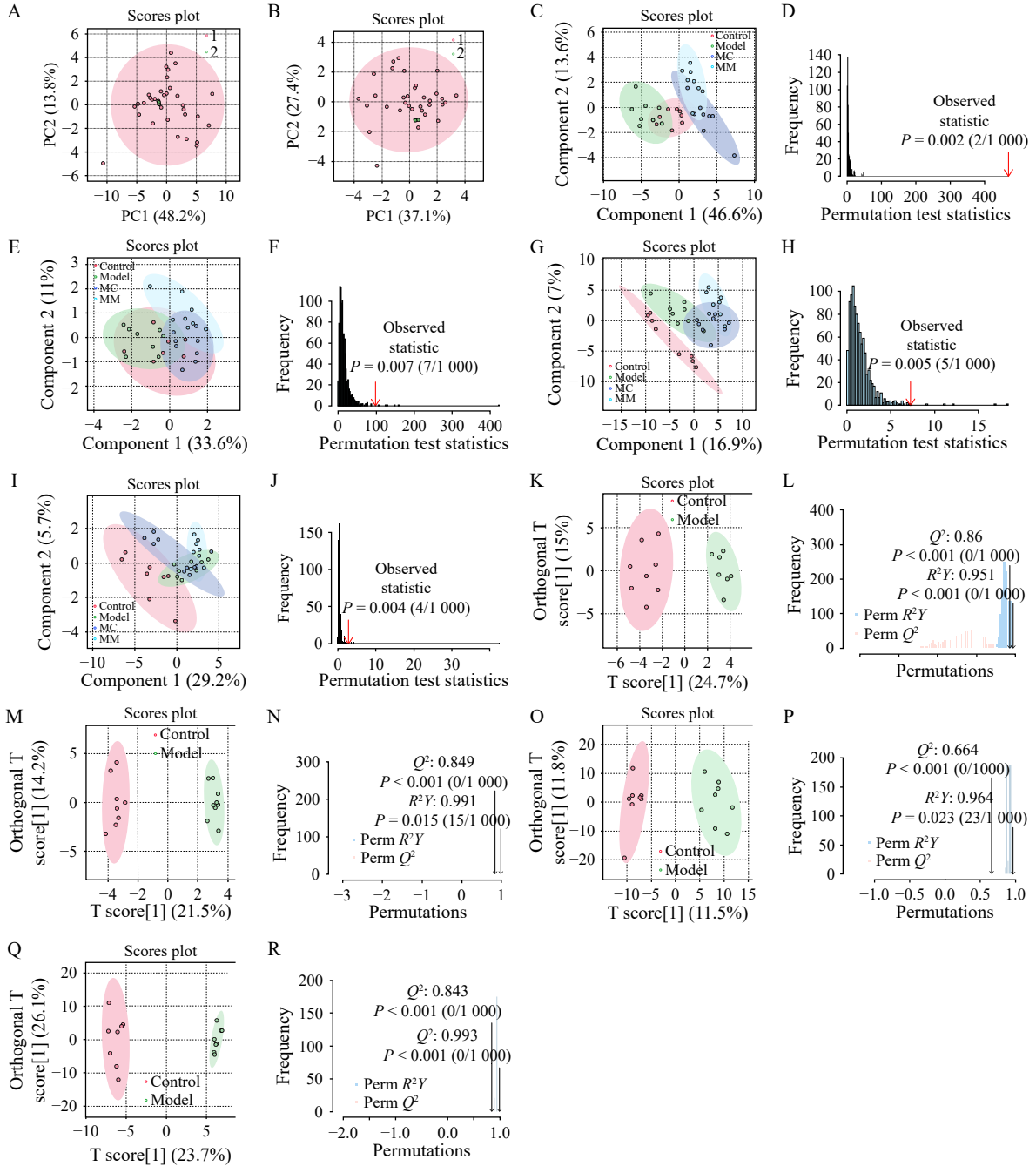

Figure 3 Integrated multivariate analysis of plasma and synovium samples with QC validation and permutation tests

A, PCA of plasma samples and QC samples in positive ion mode. B, PCA of plasma samples and QC samples in negative ion mode. C, PLS-DA score plots of plasma from each group in positive ion mode. D, permutation test result for plasma in positive ion mode (1 000 permutations, 2/1 000). E, PLS-DA score plot of plasma from each group in negative ion mode. F, permutation test result for plasma in negative ion mode (1 000 permutations, 7/1 000). G, PLS-DA score plots of synovial membrane from each group in positive ion mode. H, permutation test result for synovial membrane in positive ion mode (1 000 permutations, 5/1 000). I, PLS-DA score plots of synovial membrane from each group in negative ion mode. J, permutation test result for synovial membrane in negative ion mode (1 000 permutations, 4/1 000). K, OPLS-DA score plot for plasma in positive ion mode in model and control groups. L, permutation test result of plasma in positive ion mode. M, OPLS-DA score plot for plasma in negative ion mode in model and control groups. N, permutation test result of plasma in negative ion mode. O, OPLS-DA score plot for synovial membrane in positive ion mode in model and control groups. P, permutation test result of synovial membrane in positive ion mode. Q, OPLS-DA score plot for synovial membrane in negative ion mode in model and control groups. R, permutation test result of synovial membrane in negative ion mode. 1, plasma samples. 2, QC samples.

up-regulated, and 7 classes of lipid metabolites, including ceramide (Cer), SM, phosphatidylcholine (PC), LPC, PE, LPE, and N-acylethanolamine (NAE), were down-regulated following moxibustion intervention.

A heatmap was drawn to visualize variations in differential metabolites across plasma and synovial membrane samples in the four groups using fold change values and hierarchical clustering (Figure 4).

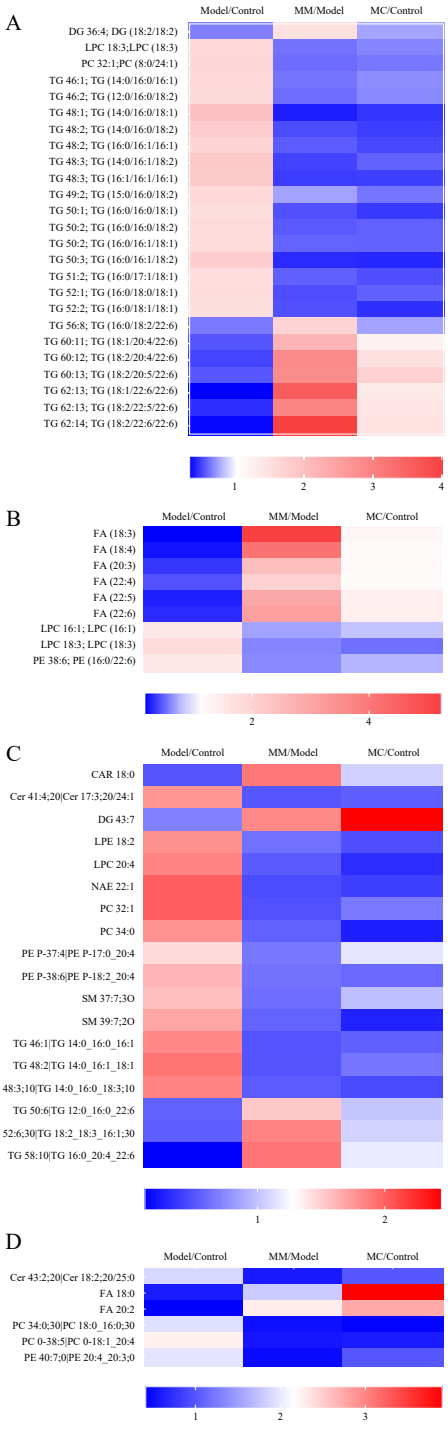

Figure 4 Heatmap analysis of differential lipid metabolites within plasma and synovial membrane in the four groups

A, differential lipids within plasma in positive ion mode. B, differential lipids within plasma in negative ion mode. C, differential lipids within synovial membrane in positive ion mode. D, differential lipids within synovial membrane in negative ion mode. Blue, downregulation. Red, upregulation.

3.4 Pathway analysis of moxibustion-regulated lipid metabolism

Metabolic pathways were analyzed to explore the potential mechanism of moxibustion intervention for RA rat models and healthy controls. Under pathological conditions (MM group vs. model group), two major metabolic pathways were identified in plasma samples: α-linolenic acid metabolism and glycerophospholipid metabolism (Figure 5A). In synovial membrane samples, three metabolic pathways were identified: α-linolenic acid metabolism, glycerophospholipid metabolism, and sphingolipid metabolism (Figure 5B). Under physiological conditions (MC group vs. control group), the glycerophospholipid metabolism pathway was identified in both plasma (Figure 5C) and synovial membrane samples (Figure 5D). Additionally, the α-linolenic acid metabolism pathway was identified in synovial membrane samples (Figure 5D).

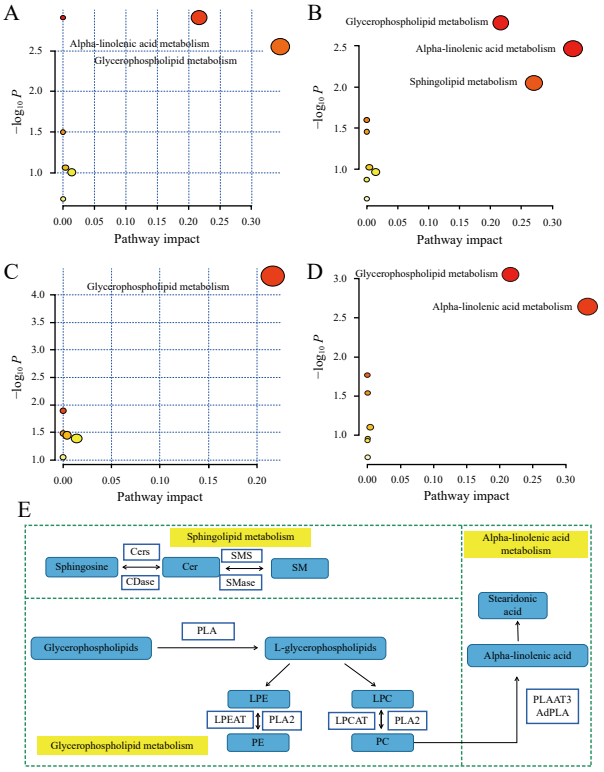

Figure 5 Bubble diagram and network diagrams of metabolic pathways in plasma and synovial membrane samples regulated by moxibustion

A, comparison of metabolic pathways in plasma between MM and model groups in pathological conditions. B, comparison of metabolic pathways in plasma between MC and control groups in physiological conditions. C, comparison of metabolic pathways in synovial membrane between MM and model groups in pathological conditions. D, comparison of metabolic pathways in synovial membrane between MC and control groups in physiological conditions. E, network diagram of main metabolic pathways involved in moxibustion treatment of RA. SMS, sphingomyelin synthase. SMase, sphingomyelinase. PLA, phospholipase A. LPEAT, lysophosphatidylethanolamine acyltransferase. LPCAT, lysophosphatidylcholine acyltransferase. PLA2, phospholipase A_2. PLAAT3, phospholipase A and acyltransferase 3. AdPLA, adipose - specific phospholipase A.

The identification of these pathways was based on the criteria of pathway impact > 0.1 and $-\log_{10} P > 2$. The

network diagram of the key pathways (Figure 5E) further elucidated the potential mechanisms of moxibustion intervention in the treatment of RA rat models. These pathways not only provide key clues for understanding the underlying mechanism of moxibustion intervention in RA treatment but also offer potential biomarkers and therapeutic targets for future research.

4 Discussion

RA, a systemic autoimmune disorder marked by chronic synovitis, joint destruction, bone loss, and systemic complications, is increasingly linked to dysregulated lipid metabolism, which contributes to its pathogenesis and progression [19, 20]. Advances in multi-omics technologies have opened new avenues for deciphering the mechanisms of TCM, including moxibustion, in modulating RA [21]. This study is the first comprehensive investigation of lipid metabolomics profiles of both plasma and synovial membrane samples in CIA rat models treated with moxibustion. Plasma was prioritized over serum for lipidomics analysis due to its reduced susceptibility to coagulation-related artifacts, ensuring more reliable biomarker identification [22]. Our findings revealed that moxibustion's therapeutic effects in pathological states were mediated through modulation of α-linolenic acid metabolism, glycerophospholipid metabolism, and sphingolipid metabolism. In contrast, under physiological conditions, its activity centered on α-linolenic acid metabolism and glycerophospholipid metabolism.

4.1 Therapeutic mechanism of moxibustion

4.1.1 α-Linolenic acid metabolism α-Linolenic acid metabolism plays an important role in the pathogenesis of RA. α-Linolenic acid and its metabolites could inhibit the activation of pro-inflammatory transcription factor NF-κB, a prominent transcription factor mitigating inflammatory responses and reducing the levels of IL-6 and TNF-α in RA patients [23, 24]. These metabolites could reduce the production of pro-inflammatory eicosanoids by competing with arachidonic acid for enzymatic conversion and directly inhibit the synthesis and release of pro-inflammatory cytokines, including IL-6 and TNF-α [25]. Additionally, they could promote the production of specialized pro-resolving mediators (SPMs), which further decrease the levels of IL-6 and TNF-α [26, 27]. In the current study, the levels of fatty acids associated with α-linolenic acid metabolism were significantly downregulated in the model group when compared to the control group, indicating a metabolic α-linolenic acid disorder in CIA rats, which is consistent with previous studies [28, 29]. Moxibustion intervention significantly upregulated the levels of these metabolites, indicating its potential to reduce the levels of TNF-α and IL -6 in plasma by regulating the abnormal metabolism of α-linolenic acid [30], thereby improving the joint symptoms in RA rat models. These findings highlight the potential therapeutic role of moxibustion in modulating lipid metabolism in RA patients.

4.1.2 Glycerophospholipid metabolism Accumulating evidence indicates that abnormal glycerophospholipid metabolism is closely associated with inflammatory processes [31, 32]. Glycerophospholipids, such as PC, PE, and LPC, are not only major components of cell membranes but also important signaling molecules involved in inflammation-induced immune responses [32]. These lipids are closely related to key inflammatory cytokines, including TNF-α and IL-6. In the glycerophospholipid metabolism pathway, the TNF signaling pathway is particularly involved in the conversion of PC to LPC, which further promotes the inflammatory process [33, 34]. In RA, this metabolic pathway elevates the level of IL-6 through reducing 1-oleoyl-sn-glycero-3-phosphocholine (OGPC) [35].

In the current study, we observed significant disturbances in glycerophospholipid metabolism in RA rat models, with lipid biomarkers primarily identified in the PC, PE, LPC, and LPE subgroups. LPC, in particular, can aggravate inflammation and disrupt osteoblast homeostasis, contributing to the development of inflammatory diseases like RA [36]. Previous study has shown that the ratio of PC/LPC in plasma is a reliable measure of inflammation and can serve as an early indicator for RA [37]. Acupuncture has been reported to alleviate inflammatory responses by regulating glycerophospholipid metabolism [38].

In our study, glycerophospholipid metabolism was significantly disrupted in model group compared with control group, with several key metabolites (including LPC, PC, and PE) showing marked upregulation. These findings are consistent with previous studies [39] and highlight the role of abnormal glycerophospholipid metabolism in the pathogenesis of RA. In addition, they also underscore the role of abnormal glycerophospholipid metabolism in RA patients. Moxibustion treatment effectively decreased the levels of these metabolites, suggesting its therapeutic efficacy in improving glycerophospholipid pathway and alleviating clinical symptoms in RA rat models.

4.1.3 Sphingolipid metabolism Sphingolipids, as a class of bioactive lipids including Cer, SMs, and lactosylceramides, are involved in multiple pathophysiological functions, encompassing the mediation of inflammatory responses through regulating cytokine and cellular signal transduction [40, 41]. Additionally, imbalance between osteoblasts and osteoclasts can lead to bone-related diseases, for instance, RA. However, sphingolipids can help maintain balance between the two [42]. Cer plays a key role in regulating inflammation and is associated with the activation of NF-κB, which is produced within local inflammatory foci or elsewhere [43, 44]. The activation of NF-κB promotes the expression of pro-inflammatory cytokines

such as IL-6 and TNF-α, which damage articular cartilage as a result [45]. This is consistent with the increased levels of IL-6 and TNF-α observed in model group in this study.

Cer is a central molecule and an important second messenger in the sphingomyelin signaling pathway, closely related to the activation of the sphingolipid signaling pathway. SMase converts SM to Cer, a process that can increase the generation of mitochondrial reactive oxygen species (ROS) through oxidative stress [46]. Oxidative stress is associated with the formation of Cer and other sphingolipids and is involved in the pathophysiology of RA [47].

In the current study, we observed significant disturbances in sphingolipid metabolism in CIA rat models, with several key sphingolipids showing marked upregulation. These changes are closely related to the pathogenesis of RA. Moxibustion effectively regulated the levels of these sphingolipids. Similar findings have been reported in the synovial fluid of RA patients and in human osteoarthritic synoviocytes, where the levels of SM and Cer were elevated compared with normal controls but restored to normal levels after treatment [48, 49]. These results highlight the potential role of sphingolipid metabolism in RA and the therapeutic efficacy of moxibustion in regulating this metabolic pathway.

Overall, moxibustion significantly modulated the expression levels of metabolic components involved in α-linolenic acid metabolism, glycerophospholipid metabolism, and sphingolipid metabolism, underscoring its potential as a therapeutic intervention for RA by targeting key metabolic pathways.

4.2 Health-promoting mechanisms of moxibustion

Despite its widespread use in TCM, the mechanisms by which moxibustion modulates lipid metabolism under physiological conditions remain underexplored. This study shows that moxibustion primarily engages two metabolic pathways: α-linolenic acid metabolism and glycerophospholipid metabolism. These findings align with prior work demonstrating moxibustion's ability to regulate lipid and energy metabolism in peripheral tissues, such as gastric mucosa under physiological conditions [50]. Moxibustion's systemic effects may arise through multiple interconnected mechanisms: by regulating autonomic nervous activity, moxibustion restores homeostasis, indirectly influencing lipid metabolism and energy balance [51]. It restores immune function, thereby enhancing host resistance by exerting bidirectional immunoregulatory effects, suppressing excessive inflammation while bolstering defense mechanisms [52]. Critically, our data demonstrated that moxibustion altered the levels of PC and LPC metabolites related to the glycerophospholipid metabolism pathway in the control group. This suggested that moxibustion fine-tuned membrane synthesis, cellular recognition, and signal transduction through the metabolism of glycerophospholipids under physiological conditions. In summary, moxibustion has important regulatory effects on lipid metabolism in hosts under physiological conditions, highlighting its potential as a health-promoting intervention.

4.3 Limitations and future research directions

The limitations of this study included the following. First, while our lipidomics approach identified key metabolic alterations in RA rat models, the exclusive reliance on lipidomic profiling may overlook interactions with other molecular pathways. Future investigations should employ integrated multi-omics strategies (e.g., proteomics, transcriptomics) to establish cross-platform metabolic networks, complemented by functional validation experiments to confirm mechanistic links. In addition, future studies should expand biofluid analysis (such as urine samples) to map systemic metabolic networks. Such efforts will deepen our understanding of moxibustion's dual regulatory effects (balancing physiological homeostasis and counteracting pathological cascades) in RA, ultimately guiding the development of personalized, mechanism-driven therapies. Second, the experimental design lacked critical control groups including non-heat stimulated skin areas, sham moxibustion (placebo) groups, and standard drug-treatment positive controls. Incorporating these controls in subsequent studies would strengthen the specificity of observed treatment effects. Finally, the mechanism of moxibustion in the physiological state remains unclear, and further studies should be conducted to explore how moxibustion regulates physiological processes in the body.

5 Conclusion

This study employed lipidomics profiling to explore the therapeutic mechanism of moxibustion in the treatment of RA, demonstrating its efficacy in ameliorating lipid metabolic dysregulation in CIA rat models. By rectifying imbalances in key lipid classes and modulating critical pathways, moxibustion attenuates inflammation and restores metabolic homeostasis, providing a mechanistic foundation for its clinical application in RA management. These findings not only validate moxibustion's traditional use but also unveil novel therapeutic targets for RA, bridging TCM with precision metabolomics.

Fundings

National Natural Science Foundation of China (81774383), Major Project of Philosophy and Social Science Research in Colleges and Universities of Jiangsu

Province (2020SJA0335), and Graduate Research and Innovation Projects of Jiangsu Province (SJCX23_0735).

Competing interests

The authors declare no conflict of interest.

References

[1] SMOLEN JS, ALETAHA D, MCINNES IB. Rheumatoid arthritis. The Lancet, 2016, 388(10055): 2023–2038.

[2] COLLABORATORS G2RA. Global, regional, and national burden of rheumatoid arthritis, 1990 – 2020, and projections to 2050: a systematic analysis of the Global Burden of Disease Study 2021. The Lancet Rheumatology, 2023, 5(10): e594–e610.

[3] MIN HK, KIM SH, KIM HR, et al. Therapeutic utility and adverse effects of biologic disease-modifying anti-rheumatic drugs in inflammatory arthritis. International Journal of Molecular Sciences, 2022, 23(22): 13913.

[4] LU MC, LIVNEH H, CHIU LM, et al. A survey of traditional Chinese medicine use among rheumatoid arthritis patients: a claims data-based cohort study. Clinical Rheumatology, 2019, 38(5): 1393–1400.

[5] ZHONG YM, ZHANG LL, LU WT, et al. Moxibustion regulates the polarization of macrophages through the IL-4/STAT6 pathway in rheumatoid arthritis. Cytokine, 2022, 152: 155835.

[6] ZENG L, GUO J, DU P, et al. Transcriptome sequencing reveals core regulation modules and gene signatures of Zusanli acupoints in response to different moxibustion warm stimulation in adjuvant arthritis rat. Hereditas, 2022, 159(1): 15.

[7] ZHONG YM, CHENG B, ZHANG LL, et al. Effect of moxibustion on inflammatory cytokines in animals with rheumatoid arthritis: a systematic review and meta-analysis. Evidence-Based Complementary and Alternative Medicine, 2020, 2020: 6108619.

[8] TAO SY, WANG X, LIAO CX, et al. The efficacy of moxibustion on the serum levels of CXCL1 and β-EP in patients with rheumatoid arthritis. Pain Research & Management, 2021, 2021: 7466313.

[9] LÜ SW, WANG QS, LI GY, et al. The treatment of rheumatoid arthritis using Chinese medicinal plants: from pharmacology to potential molecular mechanisms. Journal of Ethnopharmacology, 2015, 176: 177–206.

[10] LI YY, LV DY, LIU R, et al. Non-target metabolomic analysis reveals the therapeutic effect of *Saposhnikovia divaricata* decoction on collagen-induced arthritis rats. Journal of Ethnopharmacology, 2021, 271: 113837.

[11] SONG JY, XIANG S, YANG Y, et al. Assessment of follicular fluid metabolomics of polycystic ovary syndrome in kidney Yang deficiency syndrome. European Journal of Integrative Medicine, 2019, 30: 100944.

[12] FERREIRA HB, MELO T, PAIVA A, et al. Insights in the role of lipids, oxidative stress and inflammation in rheumatoid arthritis unveiled by new trends in lipidomic investigations. Antioxidants, 2021, 10(1): 45.

[13] SAKURABA K, KRISHNAMURTHY A, SUN JT, et al. Autoantibodies targeting malondialdehyde-modifications in rheumatoid arthritis regulate osteoclasts via inducing glycolysis and lipid biosynthesis. Journal of Autoimmunity, 2022, 133: 102903.

[14] YAN JH, YANG SS, HAN L, et al. Dyslipidemia in rheumatoid arthritis: the possible mechanisms. Frontiers in Immunology, 2023, 14: 1254753.

[15] LUAN HM, GU WJ, LI H, et al. Serum metabolomic and lipidomic profiling identifies diagnostic biomarkers for seropositive and seronegative rheumatoid arthritis patients. Journal of Translational Medicine, 2021, 19(1): 500.

[16] SOUTO-CARNEIRO M, TÓTH L, BEHNISCH R, et al. Differences in the serum metabolome and lipidome identify potential biomarkers for seronegative rheumatoid arthritis versus psoriatic arthritis. Annals of the Rheumatic Diseases, 2020, 79(4): 499–506.

[17] LENG YF, HE J, LI C, et al. Urinary metabolomics reveals the therapeutic mechanism of moxibustion on collagen-induced arthritis in rats. European Journal of Integrative Medicine, 2020, 37: 101160.

[18] LI Z. Experimental Acupuncture Science. 2008/07/26 ed. Beijing: China Press of Traditional Chinese Medicine, 2003.

[19] SPARKS JA. Rheumatoid arthritis. Annals of Internal Medicine, 2019, 170(1): ITC1–ITC16.

[20] ROCHA B, CILLERO-PASTOR B, RUIZ-ROMERO C, et al. Identification of a distinct lipidomic profile in the osteoarthritic synovial membrane by mass spectrometry imaging. Osteoarthritis and Cartilage, 2021, 29(5): 750–761.

[21] PAN HD, ZHENG YF, LIU ZQ, et al. Deciphering the pharmacological mechanism of Guan-Jie-Kang in treating rat adjuvant-induced arthritis using omics analysis. Frontiers of Medicine, 2019, 13(5): 564–574.

[22] LIU XY, HOENE M, WANG XL, et al. Serum or plasma, what is the difference? Investigations to facilitate the sample material selection decision making process for metabolomics studies and beyond. Analytica Chimica Acta, 2018, 1037: 293–300.

[23] TANG M, GAO X, GENG T, et al. Metabolomics analysis of the therapeutic effects of Qiwei Tongbi Oral Liquid on rheumatoid arthritis in rats. Journal of Pharmaceutical and Biomedical Analysis, 2021, 202: 114166.

[24] LIU YQ, ZHANG BX, CAI Q. Study on the pharmacodynamics and metabolomics of five medicinal species in *Atractylodes* DC. on rats with rheumatoid arthritis. Biomedicine & Pharmacotherapy, 2020, 131: 110554.

[25] LAZZARIN T, MARTINS D, BALLARIN RS, et al. The role of omega-3 in attenuating cardiac remodeling and heart failure through the oxidative stress and inflammation pathways. Antioxidants, 2023, 12(12): 2067.

[26] LAVY M, GAUTTIER V, POIRIER N, et al. Specialized pro-resolving mediators mitigate cancer-related inflammation: role of tumor-associated macrophages and therapeutic opportunities. Frontiers in Immunology, 2021, 12: 702785.

[27] LAMPOVA B, DOSKOCIL I, KOURIMSKA L, et al. N-3 polyunsaturated fatty acids may affect the course of COVID-19. Frontiers in Immunology, 2022, 13: 957518.

[28] XIANG FF, NIU HJ, YAO L, et al. Exploring the effect of the Uyghur medicine Munziq Balgam on a collagen-induced arthritis rat model by UPLC-MS/MS-based metabolomics approach. Journal of Ethnopharmacology, 2023, 310: 116437.

[29] YAN GL, ZHANG AH, SUN H, et al. Dissection of biological property of Chinese acupuncture point Zusanli based on long-term treatment via modulating multiple metabolic pathways. Evidence-Based Complementary and Alternative Medicine, 2013, 2013: 429703.

[30] LIANG YL, ZHANG ZF, LV TY, et al. Moxibustion at CV 8 alleviates the myocardial inflammatory response in rats with long-term exercise-induced fatigue through inhibition of the p38 MAPK/NF-κβ signaling pathway. Acupuncture & Electro-Therapeutics Research, 2020, 45(1): 31–38.

[31] CHEN TT, ZHU ZM, DU QQ, et al. A skin lipidomics study reveals the therapeutic effects of tanshinones in a rat model of acne. Frontiers in Pharmacology, 2021, 12: 675659.

[32] ZHAN X, WU H, WU H. Joint synovial fluid metabolomics method to decipher the metabolic mechanisms of adjuvant arthritis and geniposide intervention. Journal of Proteome Research, 2020, 19(9): 3769–3778.

[33] SU D, LIAO LL, ZENG Q, et al. Study on the new anti-atherosclerosis activity of different herba patriniae through down-regulating lysophosphatidylcholine of the glycerophospholipid metabolism pathway. Phytomedicine, 2022, 94: 153833.

[34] MA LL, WANG J, MA L, et al. The effect of lipid metabolism disorder on patients with hyperuricemia using multi-omics analysis. Scientific Reports, 2023, 13(1): 18211.

[35] SU J, LI SL, CHEN JH, et al. Glycerophospholipid metabolism is involved in rheumatoid arthritis pathogenesis by regulating the IL-6/JAK signaling pathway. Biochemical and Biophysical Research Communications, 2022, 600: 130–135.

[36] SANTOS M, MELO T, MAURÍCIO T, et al. The non-enzymatic oxidation of phosphatidylethanolamine and phosphatidylserine and their intriguing roles in inflammation dynamics and diseases. FEBS Letters, 2024, 598(17): 2174–2189.

[37] CARLSON AK, RAWLE RA, ADAMS E, et al. Application of global metabolomic profiling of synovial fluid for osteoarthritis biomarkers. Biochemical and Biophysical Research Communications, 2018, 499(2): 182–188.

[38] ZHANG AH, YAN GL, SUN H, et al. Deciphering the biological effects of acupuncture treatment modulating multiple metabolism pathways. Scientific Reports, 2016, 6: 19942.

[39] VESELINOVIC M, VASILJEVIC D, VUCIC V, et al. Clinical benefits of n-3 PUFA and γ-linolenic acid in patients with rheumatoid arthritis. Nutrients, 2017, 9(4): 325.

[40] HANNUN YA, OBEID LM. Sphingolipids and their metabolism in physiology and disease. Nature Reviews Molecular Cell Biology, 2018, 19(3): 175–191.

[41] OGRETMEN B. Sphingolipid metabolism in cancer signalling and therapy. Nature Reviews Cancer, 2018, 18(1): 33–50.

[42] TANG Q, LIAO L, TIAN WD. The role of sphingolipid metabolism in bone remodeling. Frontiers in Cell and Developmental Biology, 2021, 9: 752540.

[43] TANIGUCHI M, OKAZAKI T. Ceramide/sphingomyelin rheostat regulated by sphingomyelin synthases and chronic diseases in murine models. Journal of Lipid and Atherosclerosis, 2020, 9(3): 380–405.

[44] POOLMAN TM, GIBBS J, WALKER AL, et al. Rheumatoid arthritis reprograms circadian output pathways. Arthritis Research & Therapy, 2019, 21(1): 47.

[45] WANG TT, HE CQ. TNF-α and IL-6: the link between immune and bone system. Current Drug Targets, 2020, 21(3): 213–227.

[46] LI LX, BAI S, ZHAO HY, et al. Dietary supplementation with naringin improves systemic metabolic status and alleviates oxidative stress in transition cows via modulating adipose tissue function: a lipid perspective. Antioxidants, 2024, 13(6): 638.

[47] DA FONSECA LJS, NUNES-SOUZA V, GOULART MOF, et al. Oxidative stress in rheumatoid arthritis: what the future might hold regarding novel biomarkers and add-on therapies. Oxidative Medicine and Cellular Longevity, 2019, 2019: 7536805.

[48] KOSINSKA MK, LIEBISCH G, LOCHNIT G, et al. Sphingolipids in human synovial fluid: a lipidomic study. PLoS One, 2014, 9(3): e91769.

[49] SLUZALSKA KD, LIEBISCH G, ISHAQUE B, et al. The effect of dexamethasone, adrenergic and cholinergic receptor agonists on phospholipid metabolism in human osteoarthritic synoviocytes. International Journal of Molecular Sciences, 2019, 20(2): 342.

[50] LIU X, SHE C, ZHONG H, et al. Effect of moxibustion at Zusanli (ST36) on metabolites of gastric tissue in rats with chronic atrophic gastritis based on metabonomics. Acupuncture Research, 2019, 44(2): 113–119.

[51] HAN K, KIM M, KIM EJ, et al. Moxibustion for treating cancer-related fatigue: a multicenter, *Assessor*-blinded, randomized controlled clinical trial. Cancer Medicine, 2021, 10(14): 4721–4733.

[52] WANG ZQ, HUANG Y, WANG D, et al. Genome-wide regulation of acupuncture and moxibustion on ulcerative colitis rats. Evidence-Based Complementary and Alternative Medicine, 2021, 2021: 9945121.

艾灸治疗胶原诱导性关节炎大鼠的血浆与滑膜脂质组学研究

文嘉旻[a], 张睿[b], 王丹文[a], 孙志岭[a*]

a. 南京中医药大学护理学院, 江苏 南京 210023, 中国
b. 南京市急救中心急救管理科, 江苏 南京 210003, 中国

【摘要】目的 通过整合血浆及滑膜脂质组学分析，探讨艾灸对胶原诱导性关节炎（CIA）模型大鼠的治疗效果，探究艾灸在类风湿关节炎（RA）中对脂质代谢的影响。**方法** 32 只雄性 SD 大鼠被随机分为 4 组：对照组、艾灸对照（MC）组、模型组和艾灸模型（MM）组，每组 8 只。通过两次免疫诱导 SD 大鼠建立 CIA 模型。在诱导 CIA 前进行足趾容积的测量。诱导完成后，评估足趾容积和关节炎指数（AI）评分。MC 组和 MM 组在双侧肾俞穴（BL23）和足三里穴（ST36）进行艾灸治疗，每个穴位 10 分钟。治疗包括 3 个疗程，每个疗程持续 6 天，疗程间间隔 1 天。每个疗程结束后评估大鼠足趾容积和 AI 评分。在 3 个疗程结束后，采集血清、血浆、滑膜组织和踝关节样本。采用酶联免疫吸附测定（ELISA）检测血清中白细胞介素（IL）- 6 和肿瘤坏死因子（TNF）-α 的水平。通过苏木精-伊红（HE）染色对踝关节组织进行组织病理学检查。同时，利用超高效液相色谱-高分辨质谱（UHPLC-Q-Exactive Orbitrap MS）对血浆和滑膜组织样本进行分析。此外，通过多元统计分析鉴定差异脂质代谢物，并利用京都基因与基因组百科全书（KEGG）通路富集分析探究艾灸调节的代谢通路。**结果** 各组大鼠初始足趾容积和 AI 评分无显著差异（$P > 0.05$）。CIA 诱导后，与对照组相比，模型组的足趾容积增大且 AI 评分升高（$P < 0.05$），而 MM 组经艾灸治疗后上述指标较模型组显著降低（$P < 0.05$）。与对照组相比，模型组中 IL-6 和 TNF-α 的水平显著升高（$P < 0.05$），但 MM 组较模型组显著下降（$P < 0.05$）。组织病理学分析显示，MM 组的软骨状况得到改善，炎症减轻。与对照组相比，CIA 大鼠的血浆中鉴定出 33 种差异脂质代谢物，滑膜中鉴定出 24 种。在这些脂质代谢物中，艾灸调节了血浆中的 31 种脂质代谢物以及滑膜中的全部 24 种脂质代谢物。病理状态下，艾灸上调甘油二酯（DG）和脂肪酸（FA）水平，下调溶血磷脂酰胆碱（LPC）、磷脂酰胆碱（PC）和磷脂酰乙醇胺（PE）水平；生理状态下则特异性降低 LPC 和 PC 水平。通路富集分析表明，艾灸在病理状态下主要影响 α-亚麻酸、甘油磷脂和鞘脂代谢，而在生理状态下，其调节主要围绕 α-亚麻酸和甘油磷脂代谢。**结论** RA 大鼠存在显著的脂质代谢紊乱。艾灸可减轻足爪肿胀、降低 AI 评分、调节炎性因子水平并部分纠正异常脂质代谢物水平。在生理和病理条件下，艾灸参与调节脂质代谢的潜在途径包括 α-亚麻酸代谢、甘油磷脂代谢及鞘脂代谢。

【关键词】脂质组学；艾灸；类风湿性关节炎；胶原诱导性关节炎；血浆；滑膜；超高效液相色谱-高分辨质谱